Comparison between the charge carrier mobilities in pentacene OFET structures as obtained from electrical characterization and potentiometry

R. Scholz, A.-D. Müller, F. Müller, I. Thurzo, B.A. Paez, L. Mancera, D.R.T. Zahn
Institut für Physik, Technische Universität Chemnitz, D-09107 Chemnitz, Germany

C. Pannemann, U. Hilleringmann
Institut für Elektrotechnik und Informationstechnik,
Universität Paderborn, Warburger Straße 100, D-33098 Paderborn, Germany

ABSTRACT

Potentiometry with a Kelvin probe atomic force microscope is used to investigate the contact resistances of pentacene OFETs, so that the injection of the charges at the source contact and their extraction at the drain contact can be distinguished from the influence of trap states on the charge transport through the accumulation channel. The samples consist of Au bottom contacts on a SiO_2 gate dielectric with a channel length of $L = 10 - 15\ \mu$m and a channel width of $W = 100\mu$m. The gate oxide is first treated by an oxygen plasma before depositing about 30 nm of pentacene under high vacuum conditions. The output characteristics are measured as a function of temperature in an evacuated cryostat, revealing temperature-activated hole transport. The potentiometry measurements are performed *ex situ* under atmospheric conditions after storing the samples in air for several weeks. At room temperature, the pentacene OFETs are dominated by the resistance at the injection contact, so that the mobility in the channel region as deduced from potentiometry is about one order of magnitude higher than the value obtained from the output characteristics. The measurements are interpreted with microscopic model calculations for the temperature-activated currents.

1. INTRODUCTION

Organic field-effect transistors have been proposed for various applications of electronic circuits, including identification tags, smart cards and all organic flexible displays. Due to the sensitivity of most organic materials to the atmospheric conditions, the performance of organic devices may degrade significantly after their preparation. As a matter of fact, the characterization of the circuits after long storage under unfavourable conditions is still a major technological issue in order to investigate the reliability and the operational lifetime [1].
Typically, active materials like pentacene are pre-purified by sublimation under high vacuum conditions. In a second step, the organic molecules are evaporated from a Knudsen cell using a pre-patterned gate insulator as a substrate. If this deposition is carried out under well controlled high vacuum conditions, the concentration of impurities in the active channel can be rather low, but after breaking the vacuum, the electrical performance degrades due to the creation of defects or impurities under atmospheric conditions. Moreover, modifications of the morphology at the interfaces to the metal contacts may result in a change of the injection barriers with time.

2. SAMPLE PREPARATION

The preparation of the organic thin film transitors (OTFTs) started on a 100 mm *p*-conducting silicon wafer, pre-cleaned with a SC1 standard cleaning procedure. First, 430 nm field oxide was grown using thermal oxidation to affirm a sufficient insulation of the later contact pads from the gate. Using a simple OTFT bottom contact structure, the substrate was directly connected as the gate electrode (Fig. 1). UV contact lithography was chosen to define the gate area which was transferred to the SiO_2 by wet chemical etching in a buffered HF solution. After resist stripping in oxygen plasma and standard cleaning SC1, a second wet oxidation step was carried out at $960\,^0$C in order to grow an electrically stable gate dielectric. Subsequently, a SiO_2 thickness of 125 nm was determined by ellipsometry. The contacts were fabricated by evaporation of 5 nm Ni onto the gate dielectric and subsequent DC-sputtering of Au on top of it, resulting in an improved adhesion of the gold contacts on the SiO_2. The structures were patterned by UV contact lithography and lift-off with ultrasonic agitation in acetone. Separated chips were bonded to a circuit board and electrically connected in the vacuum chamber for the *in situ* measurements. As the final step, the pentacene was thermally evaporated as received from the supplier (Aldrich). The deposition rate was kept at about 1 $\mathring{A}s^{-1}$ until the film reached a thickness around 30 nm. During the deposition, the sample

Organic Field-Effect Transistors IV, edited by Zhenan Bao, David J. Gundlach, Proc. of SPIE
Vol. 5940 (SPIE, Bellingham, WA, 2005) · 0277-786X/05/$15 · doi: 10.1117/12.617004

was kept under high vacuum conditions of 2×10^{-6} mbar at room temperature.

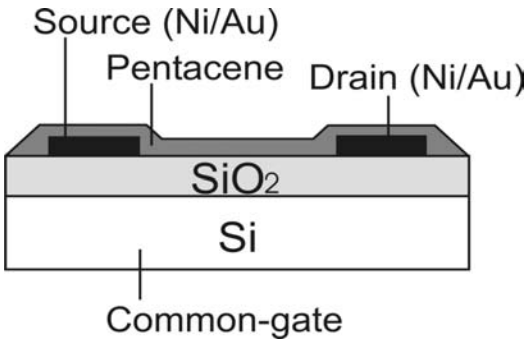

Figure 1: Schematic contact layout for the pentacene based OTFTs. The thickness of the gate oxide is about $d = 125$ nm, the channel length $L = 10 - 15$ μm, the channel width $W = 100$ μm, and the pentacene thickness 30 nm. The source and drain contacts consist of sputtered Au with a thin layer of Ni to enhance the adhesion.

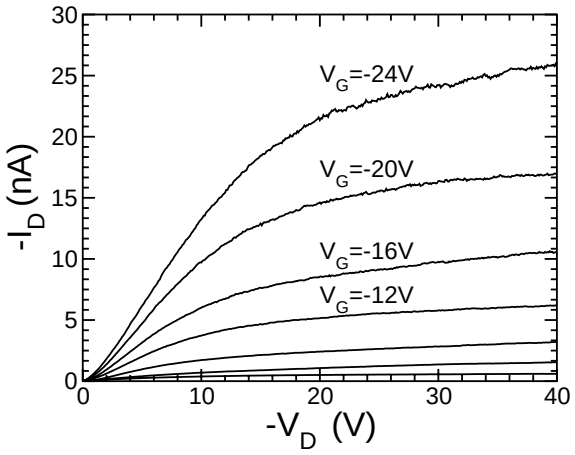

Figure 2: Output characteristics of a 30 nm thick pentacene OTFT with $L \approx 12$ μm after storing the device in air for about 8 weeks, for different gate voltages. From bottom to top: $V_G = 0, -4, -8, -12, -16, -20, -24$ V. The field effect mobility was 4×10^{-4} cm^{2}V^{-1}s^{-1} excluding the influence of a series resistance at the contacts, and 9×10^{-3} cm^{2}V^{-1}s^{-1} for a contact resistance of 0.6 GΩ.

3. ELECTRICAL CHARACTERIZATION

In principle, the preparation of the samples according to the method described above allows a full electrical characterization of the pentacene OTFTs *in situ* in high vacuum, as will be described elsewhere in more detail. For technological applications, however, the performance under atmospheric conditions is of major interest. Therefore, the objective of the present investigation was the characterization of these devices after storing them under ambient conditions for about 8 weeks.

In Fig. 2, we show the output characteristics of one of our OTFT circuits. Basing our interpretation on standard procedures [2], the drain current is given by

$$I_D = \mu C_i \frac{W}{L} V_G (V_D - I_D R_C) \tag{1}$$

where $C_i = \varepsilon_0 \varepsilon / d$ is the capacitance per area of the gate insulator of thickness d, and R_C is the contact resistance. Ignoring this contact resistance, the mobility can be derived from the linear regime $V_G < V_D < 0$ in the drain conductance,

$$g_D = \frac{\partial I_D}{\partial V_D} = \mu C_i \frac{W}{L} V_G, \tag{2}$$

resulting in a hole mobility of $\mu = 4 \times 10^{-4} \mathrm{cm}^2\mathrm{V}^{-1}\mathrm{s}^{-1}$. On the other hand, the simultaneous analysis of the drain conductance $g_D = \partial I_D / \partial V_D$ and the transconductance $g_m = \partial I_D / \partial V_G$ allows to deduce the mobility in the channel region [2],

$$\mu = \frac{g_D^2}{g_m} \frac{L}{W} \frac{V_D}{C_i V_G^2}. \tag{3}$$

Based on this formula, we obtained an estimate of $\mu = 9 \times 10^{-3}$ $\mathrm{cm}^2\mathrm{V}^{-1}\mathrm{s}^{-1}$ for the hole mobility in the accumulation channel and a contact resistance of $R_C = 0.6$ GΩ. The large influence of the contact resistance on the estimate of the mobility in the channel region indicates that a microscopic investigation of the potential drops close to the source and gate contacts would be highly desirable.

4. POTENTIOMETRY

As demonstrated earlier, potentiometry is a versatile tool allowing to determine the potential drops close to the source and drain contacts. For polymer-based field-effect transistors, it was demonstrated that the choice of the contact metals may result in rather symmetric [3] or highly asymmetric potential drops near source and gate [4]. In pentacene OTFTs, the potential drop at the source contact depends strongly on the choice of the contact metal [5].
The potentiometry measurements described in the present Section were performed in air using an atomic force microscope (AFM) built by Anfatec [6]. The AFM is equipped with a metallized tip with a radius of about 10 nm, allowing topographic measurements with less than 10 nm lateral resolution. The scans were performed with 256 scan steps of 80 nm, covering a total range of about 20 μm. The long range electrostatic contribution to the tip-substrate interaction is minimized by Kelvin probe feedback electronics adjusting the tip potential to the electrostatic potential of the underlying material. With this technique, we obtain direct insight into the electrostatic potential at the pentacene-air interface, compare Fig. 3. The data reveal a large potential drop at the source contact, depending strongly on the applied gate voltage.

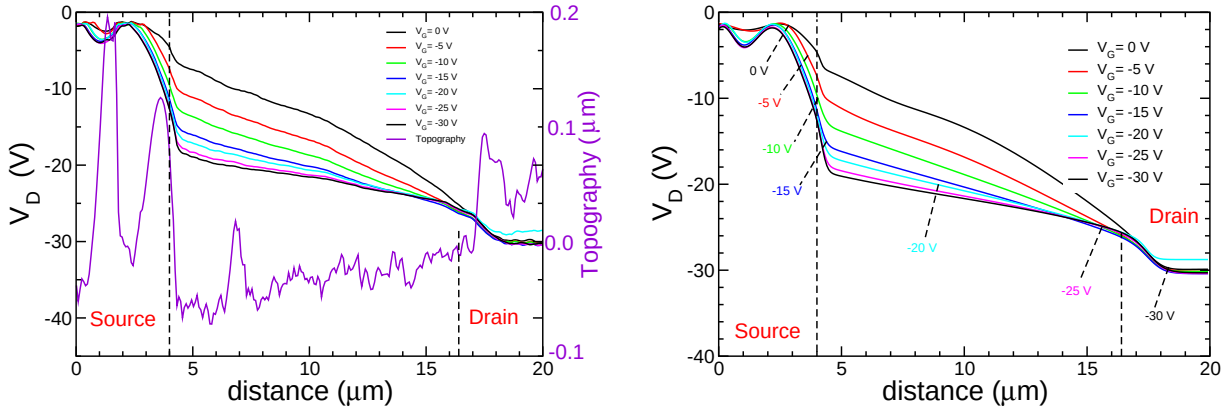

Figure 3: Left: topography and measured electrostatic potential $V(x)$ on the surface of the pentacene channel in an OTFT held at $V_D = -30$ V, for different gate voltages V_G as annoted. The data have been averaged over three consecutive scan traces at a spacing of 80 nm along the channel width. Right: interpolation of the measured potentiometry data based on a smooth function, indicating the position x_{pinchoff} where the potential in the channel coincides with the gate voltage, $V(x_{\mathrm{pinchoff}}) = V_G$.

The electric field can be deduced from a differentiation of the smooth fitting function $V_{\mathrm{fit}}(x)$ displayed on the r.h.s. of Fig. 3,

$$E_x(x) = -\frac{\partial V_{\mathrm{fit}}(x)}{\partial x}. \tag{4}$$

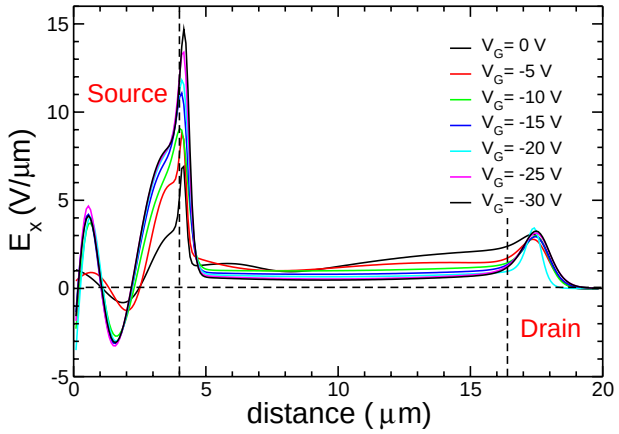

Figure 4: Electric field $E_x(x)$, as obtained from a differentation of the smooth interpolation of the measured potentiometry traces displayed in the right panel of Fig. 3.

The result is displayed in Fig. 4, revealing rather large electric fields close to the source and drain contacts together with a strongly reduced electric field in the main part of the channel. At the highest gate voltage of $V_G = -30$ V, the accumulated two-dimensional hole density can be estimated from the gate capacitance,

$$n_{2d}(x) = \frac{C_i}{q}[V(x) - V_G], \tag{5}$$

where $V(x)$ is the voltage along the channel.

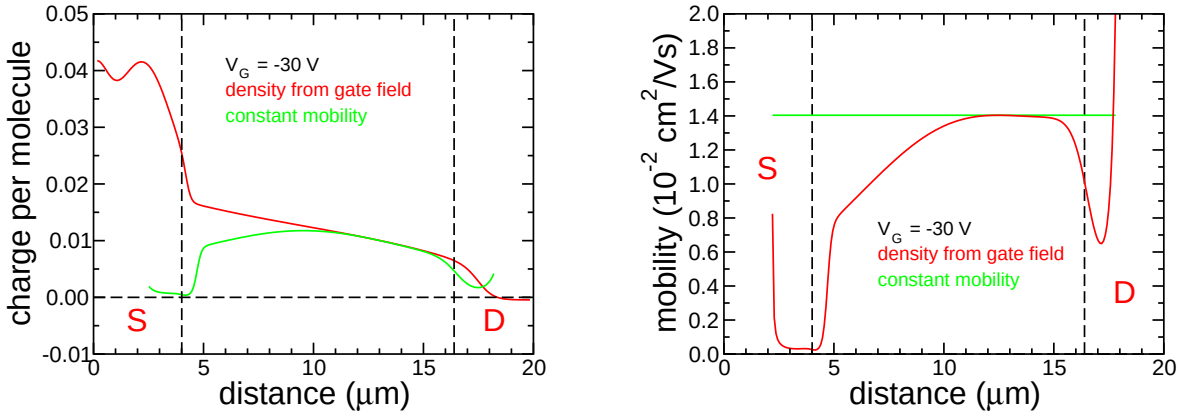

Figure 5: Left: hole density n_{3d} in the ML of pentacene closest to the gate oxide, as estimated with eqs. (5,6) from the gate capacitance (red), and hole density resulting for a constant mobility of $\mu = 1.4 \times 10^{-2}\text{cm}^2\text{V}^{-1}\text{s}^{-1}$ (green). Right: mobility of holes, for a charge density in accordance with the gate capacitance (red), and a constant mobility throughout the entire channel region (green).

Under the assumption that this charge is mainly localized in the first monolayer (ML) of pentacene on the gate dielectric [7], we can deduce the probability to find a positive charge on a molecule in this layer,

$$n_{3d}(x) = \frac{C_i}{q\, d_{\text{ML}}}[V(x) - V_G], \tag{6}$$

where $d_{\mathrm{ML}} \approx 1$ nm is the monolayer thickness. Together with the continuity of the current density,

$$\frac{I_d}{W\ d_{\mathrm{ML}}} = j(x) = e\ n_{3d}(x)\ \mu(x)\ E_x(x) = \mathrm{const}, \tag{7}$$

and the electric field $E_x(x)$ along the channel according to eq. (4), eqs. (6,7) allow the definition of a microscopic mobility, compare Fig. 5.

If the charge accumulation were governed by the gate capacitance alone, this analysis would result in a reduction of the mobility by two orders of magnitude close to the source contact. However, even though exchanging source and drain results in a reversed potential landscape, we did not find any evidence of a significant change of the drain current. Assuming again an accumulation of holes according to eqs. (5,6), the reversed potentiometry trace would lead to a different microscopic mobility under a similar electric field, a rather counter-intuitive result.

From these findings, we conclude that the quality of the pentacene is not deteriorated in some region of the channel, but merely that the hole density does not depend on the gate capacitance in the expected way.

A complementary scenario is based on a constant mobility throughout the channel, compare Fig. 5. Under this assumption, the continuity of the current density indicates a reduced hole density close to the injection contact. Therefore, contrary to the standard assumptions underlying eqs. (5,6), the gate field is not completely screened by the charge in the first ML, but it merely extends through the entire pentacene layer.

5. DEEP LEVEL TRANSIENT SPECTROSCOPY (DLTS)

In the following, we discuss the results of charge transient spectroscopy (CTS) performed on our pentacene OTFTs, a variant of DLTS where the current transient is integrated, yielding a charge transient [8,9]. It can be demonstrated that charge and current transients give complementary information with respect to the depth profiles of defect states [10]. For organic diodes based on copper phthalocyanine (CuPc), these techniques reveal a distribution of decay rates in the charge transients [11,12]. The comparison between the signature of a single decay rate with the measured distribution allows an assignment of the Gaussian broadening of the trap states, so that CTS reveals directly the density of states of the deep traps in CuPc [13].

Our DLTS traces have been obtained after switching a source-drain voltage of $V_D = 0$ to $V_D = -6$ V, with floating gate voltage. The charge transients have been recorded with the following filter function based on three consecutive measurements at the times t_1, $2t_1$ and $4t_1$ after switching the voltage:

$$\Delta Q = Q(t_1) - \frac{3}{2}Q(2t_1) + \frac{1}{2}Q(4t_1) \tag{8}$$

If each entry $Q(t)$ in eq. (8) results from the integration of a current transient with a single exponential decay time τ,

$$Q(t) = Q_0 \left[1 - \exp\left(\frac{-t}{\tau}\right)\right], \tag{9}$$

eq. (8) provides a filter for $\tau \approx t_1$. Using the filter function in eq. (8) together with a single decay constant τ according to eq. (9), we have fitted the measured CTS transients in Fig. 6, excluding data points for the longest values of t_1. The good quality of the fit demonstrates that the charge transients are dominated by a trap level with a discrete decay time τ.

If the density of states (DOS) of the trap states were broadened, the charge transient $Q(t)$ would not follow a single exponential rise as in eq. (9), resulting in turn in broadened CTS traces with respect to the fit based on eqs. (8,9). Such a behaviour was observed for polymer-based diodes [14] and for phthalocyanines [13], but for our pentacene OTFTs, we found no evidence of a broadened DOS of the trap states with a corresponding distribution of de-trapping rates.

According to Fig. 6, the decay constant τ depends on temperature, a behaviour which can be rationalized with an Arrhenius dependence for the de-trapping rate,

$$\gamma(T) = \frac{1}{\tau(T)} = \exp\left(\frac{-E_{\mathrm{act}}}{k_{\mathrm{B}}T}\right), \tag{10}$$

resulting in an activation energy of 125 ± 8 meV. This shallow trap has a much lower activation energy with respect to earlier investigations of hole traps in pentacene, where the dominating trap states where found at 0.24 eV and 0.31 eV with respect to the valence band [15].

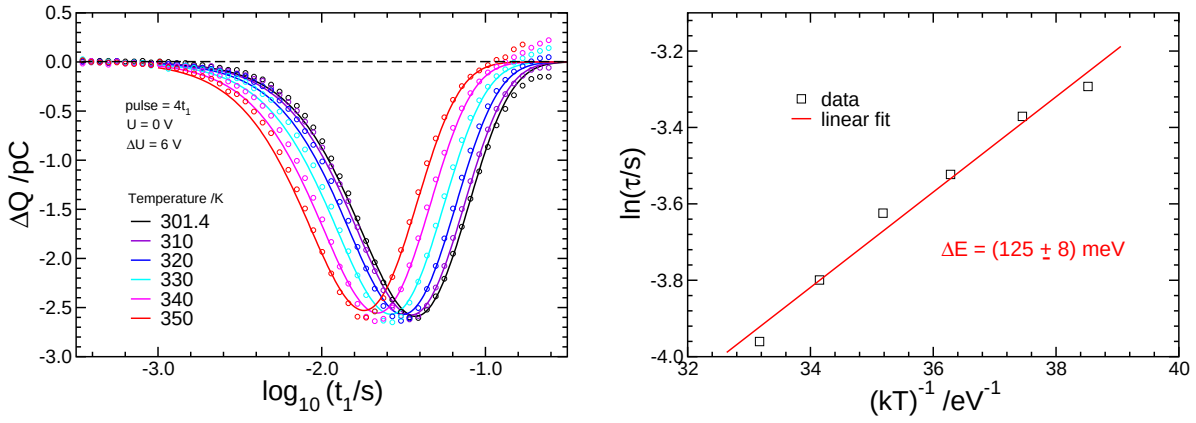

Figure 6: Left: Charge transients defined according to eq. (8) from three consecutive times t_1, $2t_1$ and $4t_1$ after switching from a voltage of $V_D = 0$ to $V_D = -6$ V, with floating gate voltage V_G. At each temperature, the measured data points are fitted according to eqs. (8,9) with a single decay constant τ. Right: Arrhenius plot of the temperature-dependent decay times according to eq. (10), revealing a trap energy of 125 ± 8 meV.

6. CHARGE DENSITIES AND BAND DIAGRAM

In Sec. 4, the analysis of the accumulation regime at $V_G = V_D = -30$ V revealed that a constant mobility of $\mu = 1.4 \times 10^{-2}\text{cm}^2\text{V}^{-1}\text{s}^{-1}$ seems to be realistic for the entire pentacene channel. Applying the same assumption to the drain current obtained at smaller gate voltages, we can deduce a hole density from each potentiometry trace, compare Fig. 7. This analysis results in a super-linear growth of the charge density with gate voltage. This finding does not contradict the linear behaviour of the drain current at low gate voltages $I_D \propto V_G$ found in Fig. 2 because the electric field E_x along the channel decreases with increasing gate voltage, compare Fig. 4. The latter effect is a direct consequence of the increase of the potential drop at the source contact at larger gate voltages.

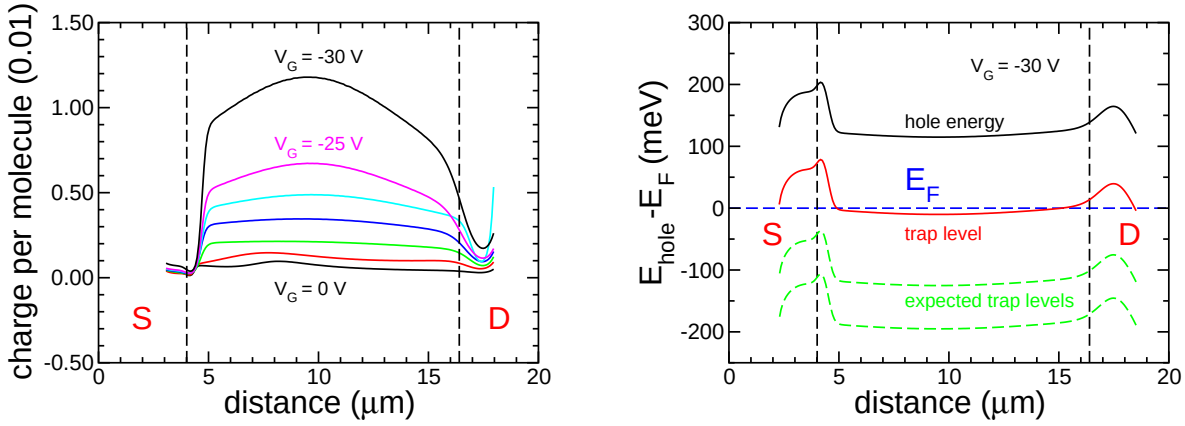

Figure 7: Left: Charge densities derived from the continuity of the current density according to eq. (7) and the electric field deduced from a smooth fit of the potentiometry traces, compare Fig. 4. Right: Position of the valence band with respect to the Fermi energy E_F, determined from the potentiometry trace obtained at $V_G = V_D = -30$ V. The trap level found with CTS is reported at 125 meV from the transport level of the holes, together with deeper trap states reported earlier for pentacene-based devices [15].

As shown in Fig. 3, at low gate voltage the pinchoff of the accumulation region is very close to the source contact. In this regime, the majority carriers cannot be accumulated at the pentacene-SiO_2 interface, and in the region with $V_D < V_G < 0$ the unscreened gate field pushes the holes to the pentacene-air interface. Therefore, at low gate voltage, the ML with the largest hole density is expected to be at the rather rough surface of the pentacene film, where the hole mobility might be smaller than at the interface between the active material and the gate dielectric.
Using Fermi-Dirac or Boltzmann statistics, the hole density can be transformed into a difference between the valence band and the Fermi energy. Moreover, the trap level found with CTS can be placed at 125 meV from the valence band, resulting in a band diagram for the relevant energy levels. The diagram obtained for $V_G = V_D = -30$ V is shown in Fig. 7, revealing that the dominating trap states are close to the Fermi energy. At smaller gate voltages, the difference between valence energy and Fermi energy increases, so that the hole traps lie above the Fermi energy. Therefore, the fraction of ionized traps increases at low gate voltage, resulting eventually in a decrease of the mobility with respect to our value of $1.4 \times 10^{-2}\mathrm{cm}^2\mathrm{V}^{-1}\mathrm{s}^{-1}$ determined in the accumulation regime at a rather high gate voltage of $V_G = V_D = -30$ V.

7. SUMMARY

In the present work it was demonstrated that the mobility deduced from the electrical characterization of pentacene OTFTs is influenced by the large contact resistances at the metal-organic interface. Potentiometry measurements with a Kelvin probe AFM have revealed a large asymmetric potential drop at the drain/source contacts going in line with a decrease of the electric field in the channel region. The continuity of the current density together with the electric field determined from the electrostatic potential allows the definition of a microscopic density of charge carriers which does not coincide with the value deduced from the gate capacitance. Instead, the poor injection at the source contact suppresses the expected hole accumulation over the first half of the channel length. A shallow trap with an energy of about 125 ± 8 meV was determined from temperature-dependent DLTS, rather close to the Fermi energy for the first monolayer of pentacene on the gate oxide. These traps result in a reduction of the expected bulk mobility by two orders of magnitude. For future pentacene-based OTFTs, the contact interface has to be designed with a smaller difference between the metal work function and the pentacene HOMO level, resulting in an improved injection. Contrary to the contact-limited OTFTs studied in the present work, such a strategy might result in a device performance defined mainly by the mobility in the channel region.

ACKNOWLEDGEMENTS

Three of us (B.A.P., L.M., and C.P.) have been supported by the Scientific Priority Programme SPP 1121 *Organic Field Effect Transistors* financed by the Deutsche Forschungsgemeinschaft.

REFERENCES

[1] C. Pannemann, T. Diekmann, and U. Hilleringmann, J. Mater. Res. **19**, 1999 (2004).
[2] G. Horowitz, R. Hajlaoui, D. Fichou, and A. El Kassmi, J. Appl. Phys. **85**, 3202 (1999).
[3] L. Bürgi, H. Sirringhaus, and R. H. Friend, Appl. Phys. Lett. **80**, 2913 (2002).
[4] L. Bürgi, T. J. Richards, R. H. Friend, and H. Sirringhaus, J. Appl. Phys. **94**, 6129 (2003).
[5] J. A. Nichols, D. J. Gundlach, and T. N. Jackson, Appl. Phys. Lett. **83**, 2366 (2003).
[6] more detailed specifications can be found under http://www.anfatec.de
[7] G. Horowitz, J. Mater. Res. **19**, 1946 (2004).
[8] J. W. Farmer, C. D. Lamp, and J. M. Meese, Appl. Phys. Lett. **41**, 1063 (1982).
[9] I. Thurzo, D. Barančok, and M. Haluška, Rev. Sci. Instrum. **66**, 5360 (1995).
[10] I. Thurzo, R. Beyer, and D. R. T. Zahn, Semicond. Sci. Technol. **15**, 378 (2000).
[11] I. Thurzo, G. Pham, and D. R. T. Zahn, Chem. Phys. **287**, 43 (2003).
[12] I. Thurzo, G. Pham, T. U. Kampen, and D. R. T. Zahn, Thin Solid Films **433**, 292 (2003).
[13] I. Thurzo, G. Pham, and D. R. T. Zahn, Semicond. Sci. Technol. **19**, 1075 (2004).
[14] A. J. Campbell, D. D. C. Bradley, E. Werner, and W. Brütting, Org. Electron. **1**, 21 (2000).
[15] Y. S. Yang, S. H. Kim, J.-I. Lee, H. Y.Chu, L.-M. Do, H. Lee, J. Oh, T. Zyung, M. K. Ryu, and M. S. Jang, Appl. Phys. Lett. **80**, 1595 (2002).